Research Article ISSN 2689-1050

Chemical & Pharmaceutical Research

Structure, Density Functional Theory, Hirshfeld Surfaces, Crystal Voids and Molecular Docking Analysis of some Estrane Derivatives

Kumari Neha and Kant Rajni*

Chemical Crystallography Laboratory, Department of Physics, University of Jammu, Jammu Tawi–180006, Jammu & Kashmir (UT), India.

***Correspondence:**
Kant Rajni, Chemical Crystallography Laboratory, Department of Physics, University of Jammu, Jammu Tawi-180006, India, Tel: +919419194375, Fax: +91 191 243 2051.

Received: 24 May 2025; **Accepted:** 02 Jul 2025; **Published:** 10 Jul 2025

Citation: Neha K. Structure, Density Functional Theory, Hirshfeld Surfaces, Crystal Voids and Molecular Docking Analysis of some Estrane Derivatives. Chem Pharm Res. 2025; 7(3): 1-8.

ABSTRACT

Estranes are a subclass of steroid, composed of eighteen carbon atoms with a gonane core. Its derivatives exhibit some notable biological properties. An attempt has been made here to investigate the crystal structure of four estrane derivatives as accessed from CSD database for their comparative crystallographic and quantum chemical analysis. These structures have been geometrically optimized using the density functional theory (DFT). The HOMO-LUMO energy gap, molecular electrostatic potential and Mulliken atomic charges have been computed using the same model. The energy band gap analysis suggested that all these structures are chemically stable. The Mulliken atomic charges and molecular electrostatic potential maps have been analyzed for the nucleophilic and electrophilic regions on the molecular surface. The three-dimensional d_{norm} plots from the Hirshfeld surface highlights the presence of C-H…O hydrogen bond interaction. The fingerprint plot analysis reveals the dominance of H…H contacts. The critical examination of crystal voids indicates the good mechanical stability for each structure. The molecular docking analysis suggests that the ligands 3-Oxoestran-17-yl acetate and 17β-Acetoxy-2β-bromo-5-methyl-5β-estran-3-one exhibit strong binding affinity towards the target protein Vitamin D_3 receptor.

Keywords

Density functional theory, Crystal voids, Estrane derivatives, Hirshfeld surfaces, Molecular docking.

Introduction

Estrane, being one of the steroid derivatives with C_{18} configuration, is a four-ring structure of which three are six-membered cyclohexane rings and one is a five-membered cyclopentane ring, with the C_{13} position allocated to the methyl group. Estrane is the basic structure of the estrogen hormone and is found essentially in males and females. The best-known estrogens that play a critical role in various physiological processes are estrone (E_1), 17β-estradiol (E_2), and estriol (E_3), respectively [1], are being the primary female sex hormone, they regulate the menstrual cycle, support reproductive health and breast development, maintain bone density and some related secondary sexual characteristics [2-4]. In males, estrogens are involved in bone maturation, sperm development, and libido regulation [5,6]. Beyond reproductive roles, estrogens contribute to cardiovascular health, skin elasticity and emotional well-being [7-9]. Imbalances in estrogen levels usually leads to significant health issues in women and the commonly manifested are in the form of osteoporosis, mood swings, hormonal disorders and cardiovascular diseases, underscoring their importance in maintaining overall physiological balance [10,11]. They also hold significant importance in medicinal chemistry and pharmacology with structural modifications influencing receptor binding affinity and selectivity [12]. These properties have led to their applications in hormone therapy, cancer treatment, and contraceptive development [13,14].

In view of the importance and diverse potential of estrane derivatives, we have identified four chemically-similar-looking estrane structures from the CSD database and are labelled as M-1: AXMESO (17β-Acetoxy-9-methyl-5α,9β,10α-estran-3-

one), M-2: CIGQEQ (3-Oxoestran-17-yl acetate), M-3 GICVET (17β-Acetoxy-2β-bromo-5-methyl-5β-estran-3-one) and M-4 ABAXES (2α-Bromo-17β-acetoxy-9-methyl-5α,9β,10α-estran-3-one) [15-17]. The crystallographic structures have been compared and the precise crystal data are presented in Table 1. The density functional theory (DFT) has been employed for all the theoretical structure analysis. The HOMO-LUMO energy gap, molecular electrostatic potential (MEP) and Mulliken atomic charges were computed using the optimized structures. The Hirshfeld surface analysis has been performed to investigate the presence of intermolecular hydrogen bond interactions. The molecular docking studies have been carried out with protein Vitamin D_3 receptor. The chemical structure of these four structures along with their atomic numbering scheme are given in Figure 1.

Table 1: Precise crystallographic details of CSD structures.

Molecule	M-1	M-2	M-3	M-4
CCDC code	AXMESO	CIGQEQ	GICVET	ABAXES
Chemical formula	$C_{21}H_{32}O_3$	$C_{20}H_{30}O_3$	$C_{21}H_{31}Br_1O_3$	$C_{21}H_{31}Br_1O_3$
Radiation used	MoKα	CuKα	CuKα	MoKα
Temperature (K)	295	293	295	295
Crystal system	Orthorhombic	Orthorhombic	Orthorhombic	Monoclinic
Space group	$P2_12_12_1$	$P2_12_12_1$	$P2_12_12_1$	$P2_1$
Cell parameters (Å, º)	a = 13.850(10)	a = 6.777(0)	a = 7.264(2)	a = 13.000(10)
	b = 12.390(10)	b = 14.074(0)	b = 8.400(1)	b = 7.380(10)
	c = 11.180(10)	c = 19.035(0)	c = 33.217(5)	c = 11.550(10)
	α, β, γ = 90º	α, β, γ = 90º	α, β, γ = 90º	α, γ = 90º, β= 115.90
Unit cell volume (Å³)	1918.4	1815.64	2026.82	996.3
Z	4	4	4	2
R-factor	0.064	0.046	0.064	0.046

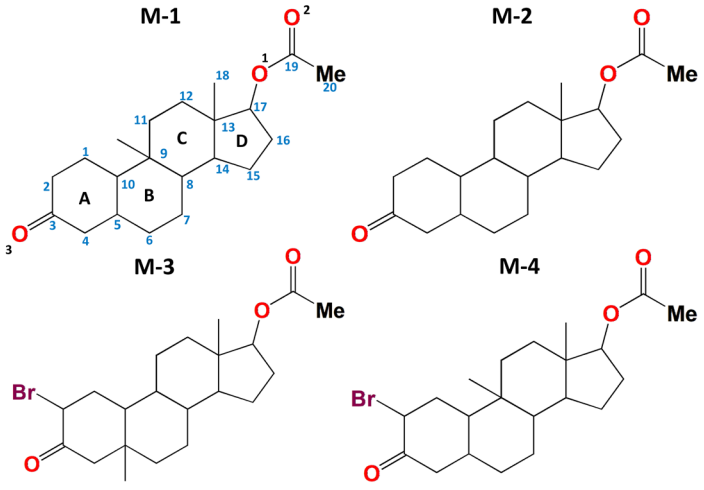

Figure 1: Chemical structure of estrane derivatives.

Quantum Chemical Calculations

All the quantum chemical computations were carried out using Gaussian 09 package [18]. The molecular geometry of each molecule was optimized via DFT, employing Becke's three-parameter functional (B3) and Lee-Yang-Parr (LYP) correlation functional with the standard 6-311++ G(d,p) basis set and the Gauss view 6 visualization software has been employed for the visual animation [19]. The individual ring conformation analysis for the estrane structure has been carried out with asymmetry parameter computation. These structures were theoretically explored in detail for the comparative investigation with the results as obtained using results of X-ray diffraction methods. Besides, HOMO/LUMO energies, molecular electrostatic potentials and Mulliken atomic charges were calculated from the output of B3LYP/6-311++G(d,p). In order to study the presence of different types of intermolecular interactions, the Hirshfeld molecular surfaces ($d_{norm,}$ shape-index, curvedness) and their corresponding 2-D fingerprint plots were generated using CrystalExplorer 21.5 [20]. The mechanical stability of each molecule has been ascertained by the crystal void analysis. The molecular docking simulation of each estrane derivative has been carried out against the Vitamin D_3 (PDB ID: 1S19) receptor using AutoDock Vina [21]. The three-dimensional structure of the target protein in *.pdb* format, was obtained from the RCSB Protein Data Bank (www.rcsb.org). Protein and ligand files were prepared in *.pdbqt* format using AutoDock Tools. The docking grid box was defined with coordinates X= 14.480, Y = 19.572 and Z = 40.776. The protein-ligand interactions were visualized using Discovery Studio software [22].

Results and Discussion

Crystallographic Analysis

The molecule M-4 exists in monoclinic crystal system with space group $P2_1$ while the molecules M-1 to M-3 crystallize in orthorhombic system with space group $P2_12_12_1$. All the structures are reportedly well refined, with R-factor ranging from 4 – 6%. The average bond lengths in rings A, B, C and D of all the identified molecules are close to 1.54Å. In addition, the average bond angle for ring A (112.21º), B (111.69º) and C (111.42º) show significant deviations from the standard value, while the average bond angle of ring D (103.68º) appears significantly deviated. The ring A, B & C exists in *chair* conformations while the ring D adopts *half-chair* conformation. The asymmetric parameters (ΔCs & ΔC_2) were calculated for each structure and the results are summarized in Table 2. The experimental and theoretically calculated bond lengths and angles have been compared and the same have been presented in the correlation graphs (Figures 2 and 3). This shows a strong correlation for M-1, M-2 and M-3 while some deviation has been found in case of M-4, and it may be attributed to the suboptimal data measurements or poor quality crystallization.

Table 2: Asymmetry parameters as calculated for individual ring system.

Ring	AXMESO (M-1)	CIGQAM (M-2)	GICVET (M-3)	ABAXES (M-4)
A	ΔCs = 3.95 ΔC_2 = 2.78	ΔCs = 3.61 ΔC_2 = 2.64	ΔCs = 1.07 ΔC_2 = 1.59	ΔCs = 1.40 ΔC_2 = 2.97
B	ΔCs = 3.57 ΔC_2 = 2.37	ΔCs = 1.34 ΔC_2 = 2.78	ΔCs = 1.84 ΔC_2 = 4.62	ΔCs = 0.76 ΔC_2 = 6.31
C	ΔCs = 2.73 ΔC_2 = 4.88	ΔCs = 4.65 ΔC_2 = 2.10	ΔCs = 3.18 ΔC_2 = 1.82	ΔCs = 5.36 ΔC_2 = 5.40
D	ΔCs = 9.85 ΔC_2 = 10.61	ΔCs = 6.81 ΔC_2 = 14.41	ΔCs = 9.95 ΔC_2 = 10.71	ΔCs = 19.10 ΔC_2 = 7.20

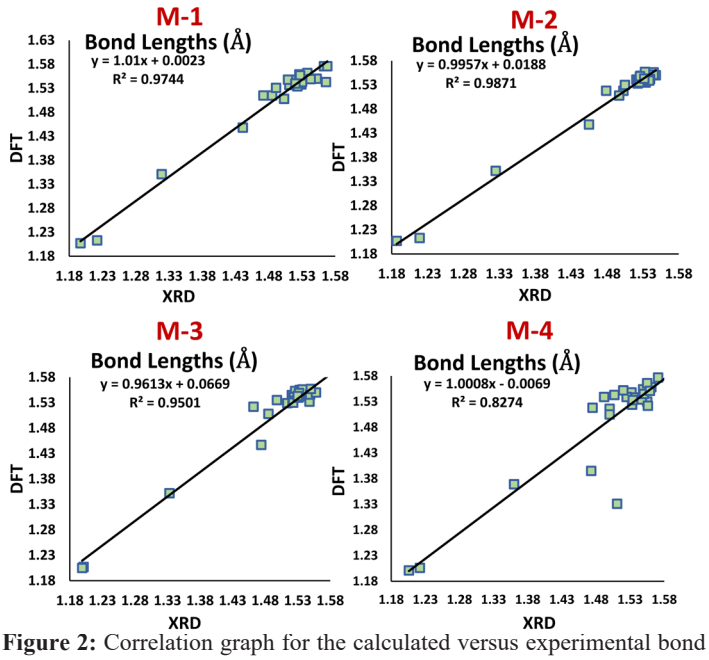

Figure 2: Correlation graph for the calculated versus experimental bond lengths.

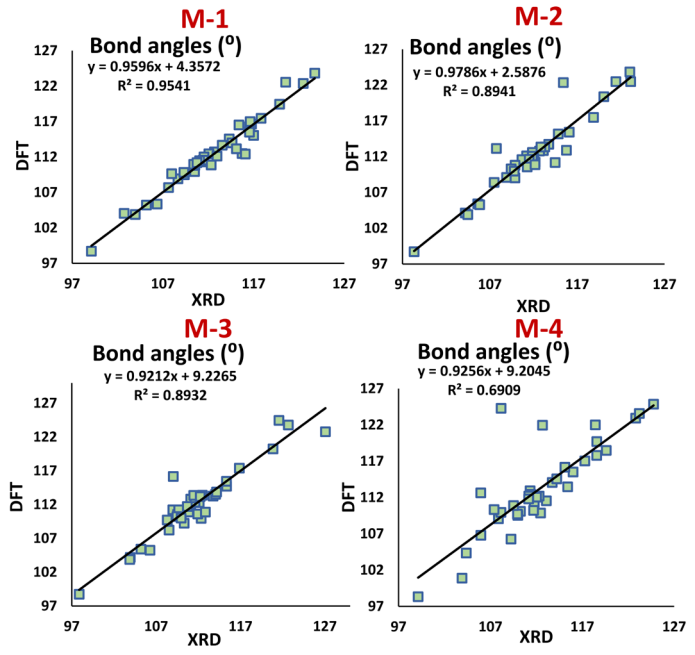

Figure 3: Correlation graph for the calculated versus experimental bond angles.

Frontier Molecular Orbital (FMO) Analysis

The analysis of frontier molecular orbitals (FMO) is crucial for assessing the chemical stability and bioactivity of a molecule [23,24]. The HOMO and LUMO energies, their energy band gaps, were calculated using B3LYP/6-311++G(d,p) level of theory. In each structure, the HOMO and LUMO orbitals are predominantly localized over the ring A and the hydroxy group (Figure 4). The FMO results for the energy band gap (ΔE_{gap}), which lies in the range of 5.95 - 6.10 eV, makes these molecules more stable and least reactive [25]. These energies, based on Koopman theorem [26], help determine some other physical parameters, viz. ionization potential (I), electron affinity (Y), chemical potential (μ), electronegativity (χ), chemical hardness (η), chemical softness (σ) and electrophilic index (ω) (Table 3). The stability and reactivity of a molecule are also characterized by its chemical potential. The negative value of the chemical potential (μ) indicates that estrane derivatives are chemically stable. The electrophilicity index, related to the biological activity of a molecule, categorizes electrophiles as strong, moderate and weak based on ω values: ω < 0.8 (weak), 0.8 < ω < 1.5 eV(moderate) and ω > 1.5(strong) [27]. In the present case, all molecules fall into the category of strong electrophiles.

Table 3: The band gap and other reactivity parameters.

Parameters	Symbols	M-1	M-2	M-3	M-4
E_{HOMO}	E_H	6.72	6.74	7.16	6.92
E_{LUMO}	E_L	0.77	0.78	1.07	1.00
Energy gap (ΔE)	$(\Delta E) = \lvert E_H - E_L \rvert$	5.95	5.96	6.09	5.92
Ionisation potential,	$I = -E_H$	-6.72	-6.74	-7.16	-6.92
Electron affinity	$Y = -E_L$	-0.77	-0.78	-1.07	-1.00
Electronegativity	$\chi = -(E_H + E_L)/2$	3.74	3.76	4.12	3.96
Chemical Potential	$\mu = -\chi$	-3.74	-3.76	-4.12	-3.96
Chemical Hardness	$\eta = \lvert E_H - E_L \rvert/2$	2.97	2.98	3.046	2.96
Chemical Softness	$\sigma = 1/2\eta\ (eV)^{-1}$	0.16	0.16	0.16	0.16
Electrophilicity	$\omega = \mu^2/2\eta$	2.35	2.37	2.78	2.64

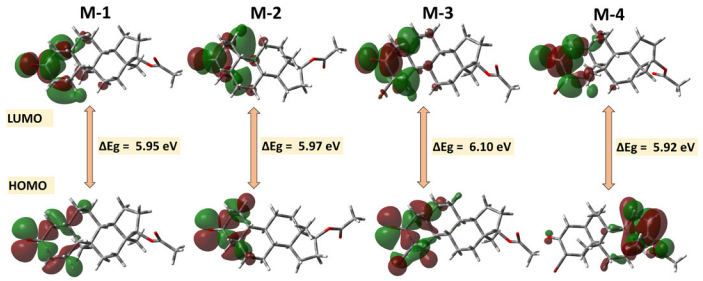

Figure 4: HOMO – LUMO energy gap of estrane derivatives.

Molecular Electrostatic Potential (MEP) and Mulliken Charge Analysis

MEP is a valuable tool for analyzing and predicting the chemically reactive regions within a molecule. It reflects the electronic density distribution and serve as an important descriptor for identifying electrophilic and nucleophilic sites as well as regions involved in hydrogen bond interactions [28,29]. It is typically visualized as a color scale in which blue signifies electron-rich (negative) region, red as electron-deficient (positive) regions, and white denotes a neutral zone [30,31]. The electron-rich regions (red and pale-yellow) in case of each structure are localized around the oxygen atoms attached at different positions, while the electron deficient regions (faint blue) are found distributed around the hydrogen atoms of the rings (Figure 5). The atomic charges for each estrane molecule have been derived from Mulliken population analysis, with optimized geometry. The magnitude of the carbon Mulliken

charge is was found to be either positive or negative, ranging from -0.901 to 0.866 (Figure 6). The highest positive and negative charges were observed for carbon atoms C_{13} = 0.866 (M-4) and C_{12} = -0.901 (M-4), respectively.

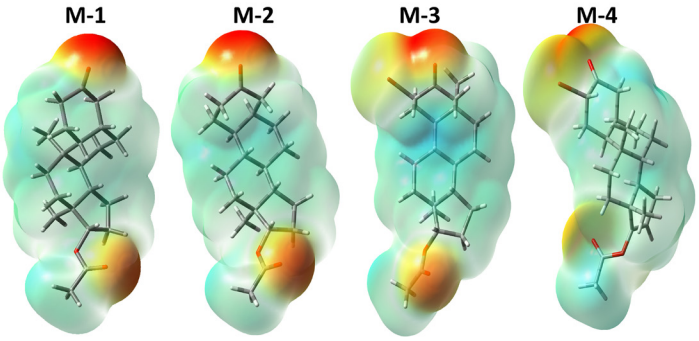

Figure 5: MEP map for estrane molecules.

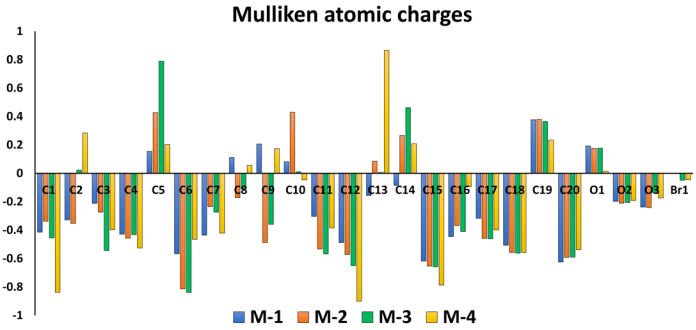

Figure 6: Mulliken atomic charges for each molecule.

Hirshfeld Surface Analysis, 2D Fingerprint Plots (FP) and Crystal Void Analysis

Hirshfeld surface analysis, a method used for investigating the physical and chemical properties of a structure, helps understand the intermolecular interactions, their nature and distribution in the crystal structure. Figure 7 illustrates the Hirshfeld surfaces mapped over d_{norm}, shape index and curvedness. The red spots on the d_{norm} maps indicate close contacts formed by C-H…O intermolecular interactions. The intermolecular interaction of the type C-H…O exists in all the molecules, the number of interactions varies, however. Besides this, the shape index and curvedness plots confirm the absence of π…π stacking interactions in all four molecules.

The 2-D fingerprint plots provide a quantitative and visual summary of the interactions in a crystal structure by analyzing the distances d_i (from the surface to the nearest atom inside the molecule) and d_e (from the surface to the nearest atom outside the molecule). The Hirshfeld surface has been plotted over the 2-D fingerprint to find the percentage contribution of each contact type to the total area (Figure 8). The summary of the contribution of individual contacts including reciprocal contacts in each estrane molecule is listed in Table 4. The major contribution to the total HS from H…H contacts is 75.9% (M-1), 76.7% (M-2), 65.3% (M-3) and 58.5% (M-4), respectively. The O…H/H…O contacts were the next major contacts which take part in the formation of C-H…O interactions. Besides, the contact between hydrogen and bromine (H…Br/Br…H) in M-3, and M-4 makes a respective contribution of 13.9% and 11.5% to the total HS. The minor contribution, of course, comes from C…H/H…C, C…O/O…C, O…Br/Br…C and C…Br/Br…C.

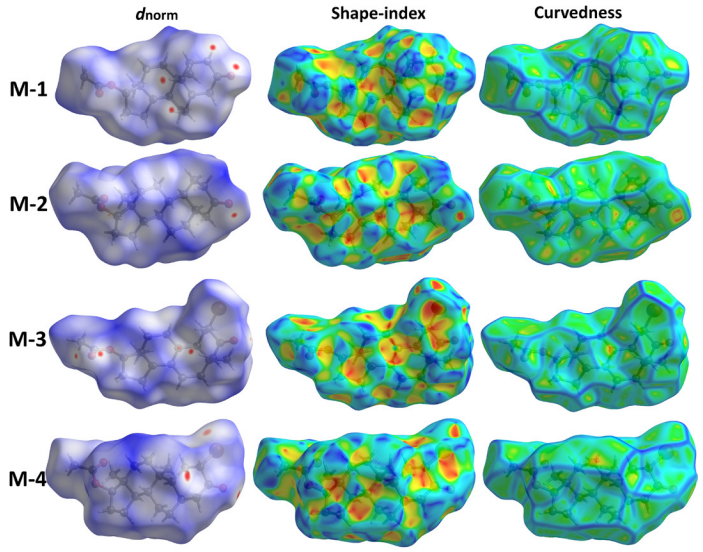

Figure 7: d_{norm}, shape index and curvedness maps.

Table 4: Percentage contribution of different contacts.

Short contacts	M-1	M-2	M-3	M-4
H-H	75.9	76.7	65.5	58.5
O-H	21.9	21.1	18.6	20.3
C-H	2.2	1.5	1.6	6.7
C-C	-	0.1	-	-
C-O	-	0.6	-	-
H-Br	-	-	13.9	11.5
O-Br	-	-	0.4	1.8
C-Br	-	-	-	1.2

The physical stability of each estrane molecule was assessed by mapping the crystal voids using a procrystal electron density isosurface (0.002 au) in Crystal Explorer 21.5 software. The crystal voids, as shown in Figure 9, reveal a void volume percentage of 16.71% for M-1, 15.59% for M-2, 16.67% for M-3 and 15.81% for M-4, respectively. These relatively similar values are indicative of the fact that all the molecules exhibit strong physical stability.

Molecular Docking

The molecular docking analysis was aimed at to assess the binding affinity and some potential pharmacological efficacy against the target protein 1S19. A comparative analysis of the docking results for estrane structures when complexed with 1S19 are present in Table 5 and Figure 10.

In **M-1:1S19** complex**,** there exists one hydrogen bond and four hydrophobic interactions. The O_2 atom of the ligand M-1 interacts with residue SER 278 at a distance of 2.98 Å, forming one

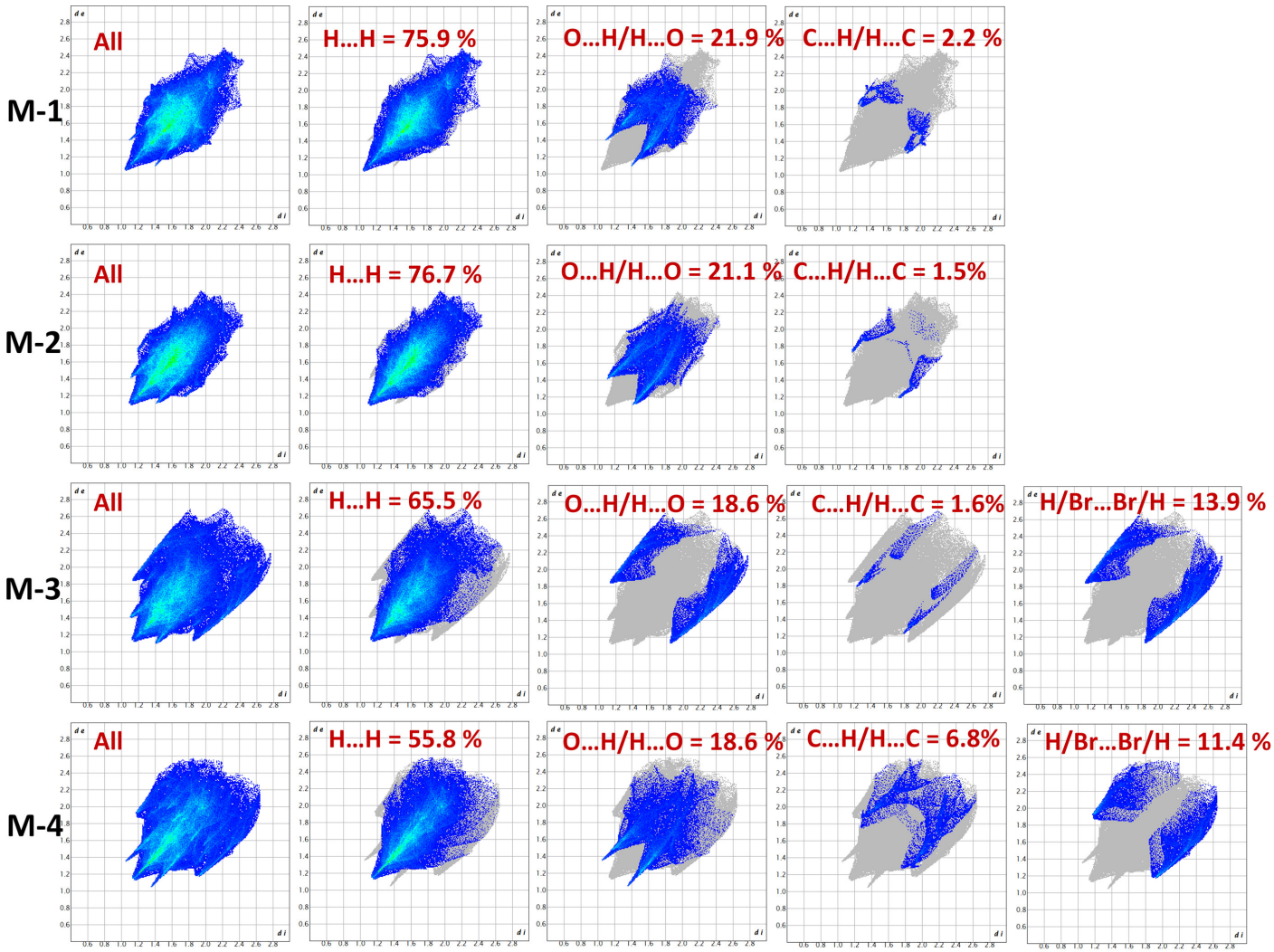

Figure 8: Fingerprint plots for estrane derivatives.

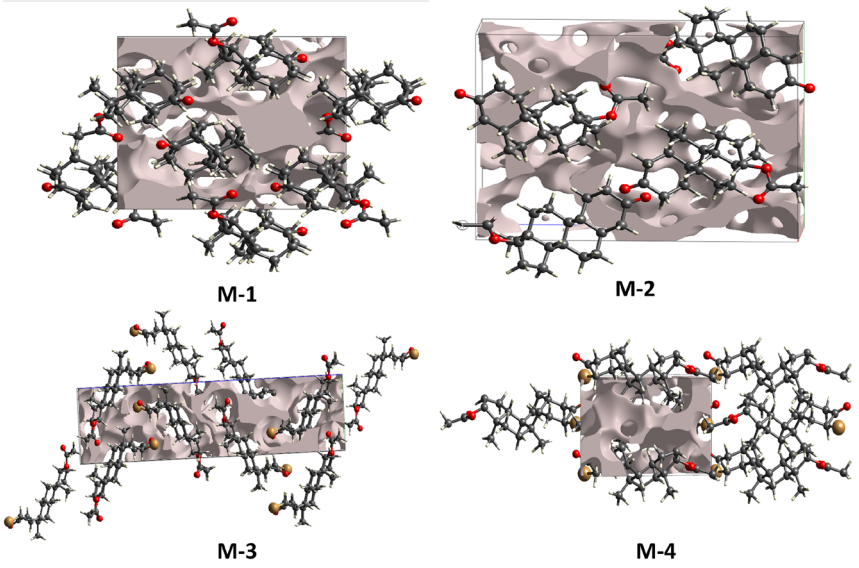

Figure 9: Void analysis for estrane derivatives

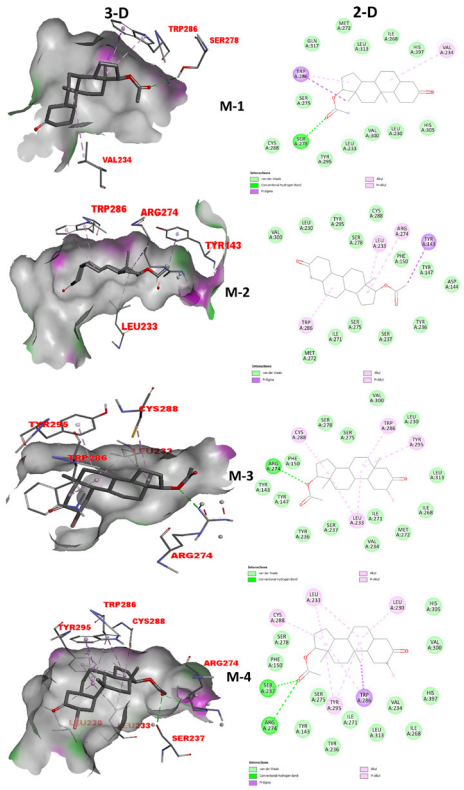

Figure 10: The three-dimensional and two-dimensional binding poses of the estrane ligands against the target protein 1S19.

Table 5: Binding score, residues, bonding interactions of estrane ligands with target protein 1S19.

Inhibitor	Binding energy (kcal mol^{-1})	Active site residue	Distance Å	Bonding	Bonding Types
M-1	-8.9	SER278	2.98	HB	Conventional HB
		TRP286	3.48	Hydrophobic	π-Sigma
		VAL234	5.50	Hydrophobic	Alkyl
		TRP286	4.74	Hydrophobic	π-Alkyl
		TRP286	4.47	Hydrophobic	π-Alkyl
M-2	-10.6	TYR143	3.72	Hydrophobic	π -Sigma
		LEU233	4.91	Hydrophobic	Alkyl
		ARG274	5.29	Hydrophobic	Alkyl
		TRP286	4.43	Hydrophobic	π-Alkyl
		TRP286	5.06	Hydrophobic	π-Alkyl
M-3	-10.1	ARG274	2.87	HB	Conventional HB
		LEU233	4.60	Hydrophobic	Alkyl
		LEU233	5.34	Hydrophobic	Alkyl
		CYS288	5.31	Hydrophobic	Alkyl
		TRP286	4.79	Hydrophobic	π-Alkyl
		TYR295	5.35	Hydrophobic	π-Alkyl
M-4	-9.1	SER237	3.34	HB	Conventional HB
		ARG274	3.31	HB	Conventional HB
		TRP286	3.94	Hydrophobic	π-Sigma
		LEU230	5.37	Hydrophobic	Alkyl
		LEU233	5.35	Hydrophobic	Alkyl
		LEU233	4.20	Hydrophobic	Alkyl
		CYS288	5.04	Hydrophobic	Alkyl
		TRP286	4.95	Hydrophobic	π-Alkyl
		TRP286	5.40	Hydrophobic	π-Alkyl
		TRP286	4.99	Hydrophobic	π-Alkyl
		TYR295	5.30	Hydrophobic	π-Alkyl
		TYR295	5.24	Hydrophobic	π-Alkyl

conventional hydrogen bond. The carbon atom C_{18} of the ligand interacts with the residue TRP286 at a distance of 3.48 Å, forming a π-sigma hydrophobic interaction. The π-orbital of ring B of the ligand M-1 interacts with the residue VAL234 at a distance of 5.50 forming an alkyl hydrophobic interaction. Besides this, two hydrophobic interactions, classified as π- Alkyl, are formed between the ring D of ligand and the residue TRP 286 at a distance of 4.74 and 4.47 Å, respectively.

For the **M-2:1S19** complex**,** there exists five hydrophobic interactions. The C_{20} atom of the ligand interacts with the residue TYR143 at a distance of 3.72 Å, forming π-sigma hydrophobic interaction. Two hydrophobic π-alkyl interactions exist between ring B of the ligand and residue TRP 286 at distances of 4.42 and 5.05 Å, respectively. Additionally, there exist two hydrophobic alkyl interactions between ring D of the ligand and residues LEU 233 and ARG 274, at distances of 4.91 Å and 5.28 Å, respectively.

The **M-3:1S19** complex gives rise to the existence one hydrogen bond and five hydrophobic interactions. The oxygen atom O_1 of the ligand M-3 interact with residue ARG 274 at a distance of 2.87Å, forming one conventional hydrogen bond. The π-orbital of ring B interact with the residue TRP 286, LEU 233 and TYR 295 at a distance of 4.79, 5.60 and 5.35 Å, respectively forming one Alkyl and two π-Alkyl hydrophobic interactions, respectively. The π-orbitals of ring D of the ligand M-3 interacts with the residue LEU233 and CYS 288 at a distance of 5.35 and 5.32 Å, respectively, forming two alkyl hydrophobic interactions.

There exist two hydrogen bonds and ten hydrophobic interactions in case of **M-4:1S19** complex. The oxygen atom O_2 of the ligand M-4 interact with two residue SER 237 and ARG 274 forming two conventional hydrogen bonds at distances of 3.34 and 3.31, respectively. The C_{19} atom of the the ligand interact with π-orbitals of residue TRP286 at a distance of 3.94 Å, forming a π-sigma hydrophobic interaction. The π-orbitals of ring B interacts with the residues LEU 230, LEU 233, TYR 295 and TRP 286 at distances of 5.37, 5.35, 5.30, 4.95 and 4.99 Å, respectively, forming two Alkyl and three π-Alkyl hydrophobic interactions. The π-orbitals of ring D interacts with residue LEU 233, CYS 288, TRP 286, TYR 295 at distances of 4.20, 5.04, 5.40 and 5.24 forming two alkyl and one π- alkyl hydrophobic interaction.

The comparison of binding energy scores indicates that M-2 and M-3 exhibit stronger binding affinities against 1S19 and therefore, may serve as more promising drug candidates for the Vitamin D_3 receptor.

Conclusions

This study encompasses theoretical investigations on the crystal structures of few estrane derivatives, including viz. DFT, Hirshfeld surface analysis and molecular docking studies. The correlation plots for bond lengths and angles in case of M-1, M-2 and M-3 show no significant deviation while there are few deviations in bond distances and angles for M-4. The HOMO-LUMO analysis suggests that the estrane molecules are chemically stable. The MEP surface analysis reveals that the electrophilic attacks are likely to happen around the O_1 and N_3 atoms, while nucleophilic attacks occur around the hydrogen atoms. The Hirshfeld surface analysis confirms the presence of C-H…O intermolecular interactions in all structures. The 2-D fingerprint plots highlight the dominance of H-H interactions. The mechanical stability of these structures is comparable and their crystal packing is densely packed. The molecular docking study of all the four molecules with protein Vitamin D_3 receptor reveals that a binding score ~ 10 kcal/mol for M-2 and M-3 may make these two molecules exhibiting strong affinity towards the target protein.

References

1. Bennink HJC. Are all estrogens the same?. Maturitas. 2004; 47: 269-275.
2. Yu Z, Jiao Y, Zhao Y, et al. Level of Estrogen in Females-The Different Impacts at Different Life Stages. J Pers Med. 2022; 12: 1995.
3. Munk AJL, Zoeller AC, Hennig J. Fluctuations of estradiol during women's menstrual cycle: Influences on reactivity towards erotic stimuli in the late positive potential. Psychoneuroendocrinology. 2018; 91: 11-19.
4. Santoro N, Worsley R, Miller KK, et al. Role of Estrogens and Estrogen-Like Compounds in Female Sexual Function and Dysfunction. J Sex Med. 2016; 13: 305-316.
5. Schulster M, Bernie A, Ramasamy R. The role of estradiol in male reproductive function. Asian J Androl. 2016; 18: 435-440.
6. Lombardi G, Zarrilli S, Colao A. Estrogens and health in males. Mol Cell Endocrinol. 2001; 178: 51-55.
7. Aryan L, Younessi D, Zargari M, et al. The Role of Estrogen Receptors in Cardiovascular Disease. Int J Mol Sci. 2020; 21: 4314.
8. Thornton MJ. Estrogens and aging skin. Dermatoendocrinol. 2013; 5: 264-270.
9. Albert KM, Newhouse PA. Estrogen, Stress, and Depression: Cognitive and Biological Interactions. Annu Rev Clin Psychol. 2019; 15: 399-423.
10. Cheng CH, Chen LR, Chen KH. Osteoporosis Due to Hormone Imbalance: An Overview of the Effects of Estrogen Deficiency and Glucocorticoid Overuse on Bone Turnover. Int J Mol Sci. 2022; 23: 1376.
11. Xiang D, Liu Y, Zhou S, et al. Protective Effects of Estrogen on Cardiovascular Disease Mediated by Oxidative Stress. Oxid Med Cell Longev 2021; 2021: 1-15.
12. Agatonovic-Kustrin S, Turner J. Molecular Structural Characteristics of Estrogen Receptor Modulators as Determinants of Estrogen Receptor Selectivity. Mini-Reviews in Medicinal Chemistry. 2008; 8: 943-951.
13. Likis FE. Contraceptive applications of estrogen. JMWH. 2002; 47:139-156.
14. Stuenkel CA. Menopausal hormone therapy and the role of estrogen. Clin Obstet and Gynecol. 2021; 64: 757-771.

15. Boeyens JCA, Bull JR, Floor J, et al. Steroidal analogues of unnatural configuration. Part 12. Ring A reactions of 9-methyl-5β,9β,10α- and 9-methyl- 5α,9β,10α-estran-3-ones: conformational analysis and X-ray crystallography of products. J Chem Soc, Perkin Trans. 1978; 1: 808-817.
16. Ramachary DB, Sakthidevi R, Reddy PS. Direct organocatalytic stereoselective transfer hydrogenation of conjugated olefins of steroids. RSC Adv. 2013; 3: 13497.
17. Van Rooyen PH. Structure of 17β-acetoxy-2β-bromo-5-methyl-5β-estran-3-one. Acta Crystallogr C. 1988; 44: 1317-1318.
18. Frisch MJ, Trucks GW, Schlegel HB, et al. Gaussian 09; Gaussian, Inc. Wallingford, CT, 2009; 32: 5648-5652.
19. Dennington R, Keith TA, Millam JM. Environmentally Friendly Room Temperature Synthesis of 1-Tetralone over Layered Double Hydroxide-Hosted Sulphonato-Salen-Nickel(II) Complex. Green and Sustainable Chemistry. 2023; 13: 9-22.
20. Spackman PR, Turner MJ, McKinnon JJ, et al. CrystalExplorer : a program for Hirshfeld surface analysis, visualization and quantitative analysis of molecular crystals. J Appl Crystallogr. 2021; 54: 1006-1011.
21. Morris GM, Huey R, Lindstrom W, et al. AutoDock4 and AutoDockTools4: Automated docking with selective receptor flexibility. J Comput Chem. 2009; 30: 2785-2791.
22. https://www.3ds.com/products/biovia/discovery-studio/visualization
23. Tariq S, Raza AR, Khalid M, et al. Synthesis and structural analysis of novel indole derivatives by XRD, spectroscopic and DFT studies. J Mol Struct. 2020; 1203: 127438.
24. AHM J, RP, RS, et al. Structural, Quantum Chemical, Molecular Docking, and Dynamics Studies of Quercetin-A Potent Inhibitor for Colon Cancer. Polycycl Aromat Compd. 2023; 43: 8426-8441.
25. Janani S, Rajagopal H, Muthu S, et al. Molecular structure, spectroscopic (FT-IR, FT- Raman, NMR), HOMO-LUMO, chemical reactivity, AIM, ELF, LOL and Molecular docking studies on 1-Benzyl-4-(N-Boc-amino) piperidine. J Mol Struct. 2021; 1230: 129657.
26. Manne R, Åberg T. Koopmans' theorem for inner-shell ionization. Chem Phys Lett. 1970; 7: 282-284.
27. Parthasarathi R, Subramanian V, Roy DR, et al. Electrophilicity index as a possible descriptor of biological activity. Bioorg Med Chem. 2004; 12: 5533-5543.
28. Palled R, Srinivasan V, Al-Asbahi BA, et al. A comprehensive investigation of ethyl 2- (3-methoxybenzyl) acrylate substituted pyrazolone analogue: Synthesis, computational and biological studies. Chemical Physics Impact. 2024; 8: 100531.
29. Koyambo-Konzapa S-J, Oubella A, Issaoui N, et al. Molecular structure, spectroscopic (FT-IR, NMR and UV–Vis), electronic properties, molecular docking, and molecular dynamics studies on novel thiazolidinone derivative: A potent breast cancer drug. J Mol Struct. 2024; 1318: 139301.
30. Oueslati Y, El Bakri Y, Valkonen A, et al. Growth, single crystal investigation, hirshfeld surface analysis, DFT studies, molecular docking, physico-chemical characterization and, in vitro, antioxidant activity of a novel hybrid complex. J Solid State Chem. 2021; 301: 122319.
31. Balachandran V, Santhi G, Karpagam V, et al. DFT computation and spectroscopic analysis of N-(p-methoxybenzylidene) aniline, a potentially useful NLO material. J Mol Struct. 2013; 1047: 249-261.